AIP Advances

Motion-induced eddy current thermography for high-speed inspection

Cite as: AIP Advances **7**, 085105 (2017); https://doi.org/10.1063/1.4997152
Submitted: 14 April 2017 • Accepted: 26 July 2017 • Published Online: 11 August 2017

Jianbo Wu, Kongjing Li, Guiyun Tian, et al.

View Online Export Citation CrossMark

ARTICLES YOU MAY BE INTERESTED IN

NDT of railway components using induction thermography
AIP Conference Proceedings **1706**, 150001 (2016); https://doi.org/10.1063/1.4940613

Physical interpretation and separation of eddy current pulsed thermography
Journal of Applied Physics **113**, 064101 (2013); https://doi.org/10.1063/1.4790866

Eddy current pulsed phase thermography and feature extraction
Applied Physics Letters **103**, 084104 (2013); https://doi.org/10.1063/1.4819475

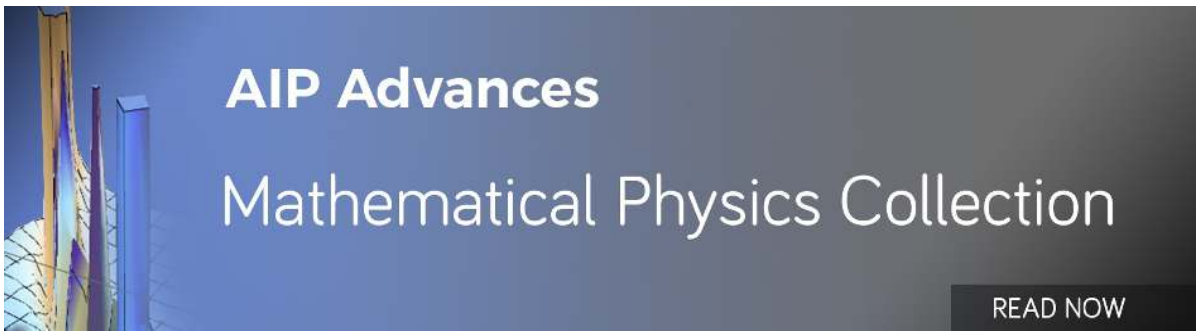

AIP Publishing

© 2017 Author(s).

Motion-induced eddy current thermography for high-speed inspection

Jianbo Wu,[1] Kongjing Li,[2] Guiyun Tian,[2,3,a] Junzhen Zhu,[2] Yunlai Gao,[2] Chaoqing Tang,[2] and Xiaotian Chen[2]
[1]*School of Manufacturing Science and Engineering, Sichuan University, Chengdu 610065, China*
[2]*School of Electrical & Electronic Engineering, Newcastle University, Newcastle upon Tyne NE1 7RU, United Kingdom*
[3]*School of Automation Engineering, University of Electronic Science and Technology of China, Chengdu 611731, China*

(Received 14 April 2017; accepted 26 July 2017; published online 11 August 2017)

This letter proposes a novel motion-induced eddy current based thermography (MIECT) for high-speed inspection. In contrast to conventional eddy current thermography (ECT) based on a time-varying magnetic field created by an AC coil, the motion-induced eddy current is induced by the relative motion between magnetic field and inspected objects. A rotating magnetic field created by three-phase windings is used to investigate the heating principle and feasibility of the proposed method. Firstly, based on Faraday's law the distribution of MIEC is investigated, which is then validated by numerical simulation. Further, experimental studies are conducted to validate the proposed method by creating rotating magnetic fields at different speeds from 600 rpm to 6000 rpm, and it is verified that rotating speed will increase MIEC intensity and thereafter improve the heating efficiency. The conclusion can be preliminarily drawn that the proposed MIECT is a platform suitable for high-speed inspection. © *2017 Author(s). All article content, except where otherwise noted, is licensed under a Creative Commons Attribution (CC BY) license (http://creativecommons.org/licenses/by/4.0/).*
[http://dx.doi.org/10.1063/1.4997152]

I. INTRODUCTION

As an emerging non-destructive testing method, eddy current thermography (ECT) combines eddy current testing and thermography with advantages such as non-contact, full-field coverage and high resolution.[1–4] In the traditional offline inspection such as for carbon fiber reinforced plastic,[5,6] propeller[7] and bond wires,[8] usually, a coil (e.g. Line-coil, Helmholtz-coil and Ferrite-yoke-coil)[9] is positioned above the inspected object. High-frequency alternative current with high amplitude passing through the coil will generate a time-varying magnetic field and then induce eddy current in the object. Based on Joule's law, heat will be generated around defects, which can be captured by infrared camera. In above applications, the excitation coil and the inspected object are both fixed, and the object can be heated as long as required since there is no testing speed restriction. Recently, high-speed ECT inspection is in great demand such as online monitoring for rail track and wheel.[9,10] When the traditional coil heating method is applied to high-speed inspection, it will face insufficient heating problem. Netzelmann developed a scanning ECT system for rail track at a maximum speed of 15 km/h.[10] It was found that the thermal contrast of defect decreases with the square root of the scanning speed due to the shortened heating time. Thus, to ensure sufficient heating for high-speed inspection, a novel ECT heating method for is required.

Different from the eddy current induced by AC coil in traditional ECT method, motion-induced eddy current (MIEC) is induced by the relative movement between magnetic field and conductive

[a]Corresponding author. E-mail: g.y.tian@newcastle.ac.uk

 © Author(s) 2017

object.[11–17] Jianbo Wu and Yong Li investigated the MIEC effect on magnetic flux leakage testing and it was found that high-speed mechanical motion of inspected object in a magnetizing field will generate strong MIEC in the specimen and further influence the testing signals.[11,12] In addition to the MIEC induced by mechanical motion, Junjun Xin used an electronic-driven way to create a rotating magnetic field in steam generator tubes to generate MIEC for material evaluation,[13,14] in which the rotating magnetic field is created by three-phase windings. And of course, according to Joule's law the MIEC will generate resistive heat in the object. MIEC heat treatment method based on moving permanent magnets was proposed.[18,19] It was verified that there is a positive correlation between moving speed and temperature increasing rate. Besides, linear eddy current brake caused the rail temperature rise with the increase of train moving speed.[20,21]

The above researches indicate that the MIEC illustrates a unique character that the moving speed will increase MIEC intensity and thereafter improve the heating efficiency, which paths a better way for high-speed inspection. To further understand this character, an experimental setup to build a high-speed relative motion between the magnetic field and inspected object is needed. The high-speed mechanical motion method has multiple influence factors such as lift-off distance change due to vibration, material inhomogeneity, motion blur of infrared image and potential risk. In this letter, to investigate the physical principle of MIEC heating and eliminate the above multiple factors, three-phase windings are applied to create a rotating magnetic field. This electronic-driven method can be easily and safely implemented without mechanical motion.

II. PRINCIPLE OF MIEC INDUCED BY ROTATING MAGNETIC FIELD

As shown in Fig. 1 (a) and (b), three identical windings are located on axes physically 120° apart, which are supplied by three-phase alternative currents A(A′), B(B′) and C(C′) with difference between the phases of 2π/3. The vector sum of the fields will generate a rotating magnetic field with four poles (i.e. two N poles and two S poles), which indicated by black dash line. According to Faraday's law, the rotating magnetic field will induce MIEC in the specimen. The MIEC density can be expressed as follow:

$$j(r) = \sigma v(r) \times B(r) \tag{1}$$

where $j(r)$, σ, $v(r)$ and $B(r)$ denote the MIEC density, the conductivity, the relative velocity and the magnetic field at position r, respectively.

The MIEC itself will also induce magnetic field, hence the magnetic field $B(r)$ in Eq. (1) consists of the external magnetic field B_{ext} generated by three-phase currents and the internal magnetic field B_{int} generated by the MIEC. According to the rotating direction of the magnetic field, only the radial component of magnetic field will generate the MIEC and the MIEC will be axially orientated. Further, the MIEC can be expressed by

$$j_a = \sigma v_t (B_{rext} + B_{rint}) \tag{2}$$

where the j_a denote the axially-orientated MIEC density; v_t denote the tangentially speed; B_{rext} and B_{rint} denote the radial components of the external and internal magnetic fields, respectively.

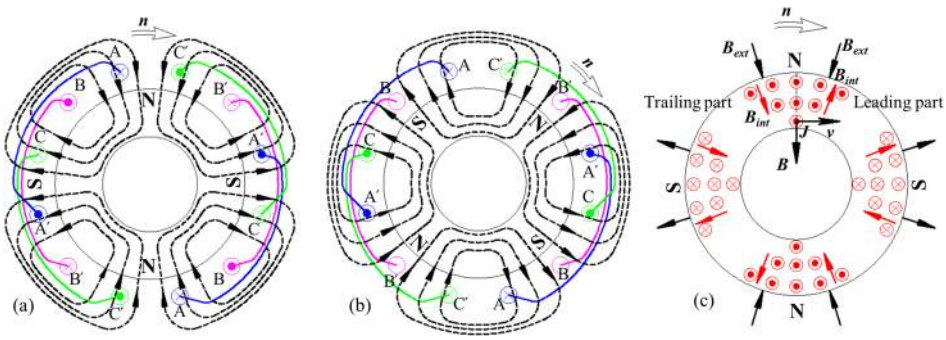

FIG. 1. MIEC induced by rotating magnetic field. (a) and (b) The rotating magnetic field distribution generated by three-phase windings; (c) the MIEC distribution generated rotating magnetic field.

As displayed in Fig. 1 (c), MIEC below the two N poles will flow outside; in contrast, these below the two S poles will flow inside. Along the rotation direction, the specimen is divided into two parts: the leading part and the trailing part. According to the Lenz's law, in the leading part, the MIEC will induce an internal magnetic field with its radial component direction different from the external magnetic field; in contrast, in the trailing part, the radial component of MIEC-induced internal magnetic field will has the same direction as the external magnetic field. Based on Eq. (2), the MIEC in the leading and trailing parts can be expressed as follows:

$$j_a\,(\mathrm{l}) = \sigma v_t\,(B_{rext} - B_{rint}) \tag{3}$$

$$j_a\,(\mathrm{t}) = \sigma v_t\,(B_{rext} + B_{rint}) \tag{4}$$

where $j_a(l)$ and $j_a(\mathrm{t})$ denote the MIEC density in the leading and trailing parts, respectively.

From the Eqs. (3) and (4), it can be concluded that more MIEC will be generated in the trailing part than in the leading part, i.e. delay effect, since the magnetic field in the trailing part is greater than that in the leading part. With the rotating speed increasing, the delay effect will be more obvious.

According to Joule's law, the power losses of MIEC convert into heat Q as follow:

$$Q = \frac{1}{\sigma}|j_a|^2 t \tag{5}$$

Based on Eq. (2), the relationship between the power losses and the moving speed is expressed by

$$Q = \frac{1}{\sigma}(\sigma v_t\,(B_{rext} + B_{rint}))^2 t = \sigma {v_t}^2 (B_{rext} + B_{rint})^2 t \tag{6}$$

From the Eq. (6), it can be concluded that increasing the moving speed will improve heating efficiency, which benefits the high-speed inspection.

Finally, the generated Joule heat diffuses inside the material. The diffusion process is governed by

$$\rho C_p \frac{\partial T\,(r,t)}{\partial t} - \nabla \cdot (k \nabla T\,(r,t)) = q\,(r,t) \tag{7}$$

where $T(r, t)$ represents the temperature of the position r at time t; the ρ, C_P, k and $q(r, t)$ denote material density, thermal capacity, thermal conductivity of material and the thermal density, respectively. Based on Eqs. (5), (6) and (7), the MIEC density, the heat and the temperature are linked to each other, forming the principle of MIECT.

III. SIMULATION OF MIEC GENERATED BY ROTATION MAGNETIC FIELD

To investigate the distribution and heating principle of MIEC, 2D numerical simulations are conducted in COMSOL. A steel hollow plate (Internal radius: 15 mm; External radius: 30 mm) is placed in the center of three-phase windings (Internal radius: 32 mm; External radius: 52 mm; Turns number: 2000). Three-phase currents (Intensity: 5A; Frequency: 1Hz) passing through the windings create a rotating magnetic field with rotating speed of 30 rpm. The magnetic flux distribution is simulated and indicated by red line in Fig. 2(a), which has four symmetrically-distributing poles. Then, the rotational motion of the magnetic field induces four MIEC in the specimen below the poles, as displayed in Fig. 2 (b). At a low rotating speed, the MIEC-induced magnetic field is weak and the delay effect can be negligible, thus MIEC in the leading and trailing parts are symmetrical. However, when magnetic field rotates at a high speed of 1500 rpm, the delay effect is obvious that more MIEC are induced in the trailing part than in the leading part, as displayed in Fig. 2(c). Besides, at a higher rotating speed, MIEC concentrates more closely to the surface, i.e. skin effect.

MIECT is based on the changed MIEC distribution caused by defects in the specimen. At different rotating speeds, the delay effect and skin effect will have different influences on the interaction of the MIEC and the defect. Due to the delay effect, from specimen surface to the inside, MIEC arrives at the defect at a different time, which will influence the heating process. Besides, at a slow speed, the MIEC has a deep penetration and most of it will be blocked by the internal defect. However, with the rotation speed increasing to a high level, the MIEC will concentrate at the surface with its flow less affected by the defect.

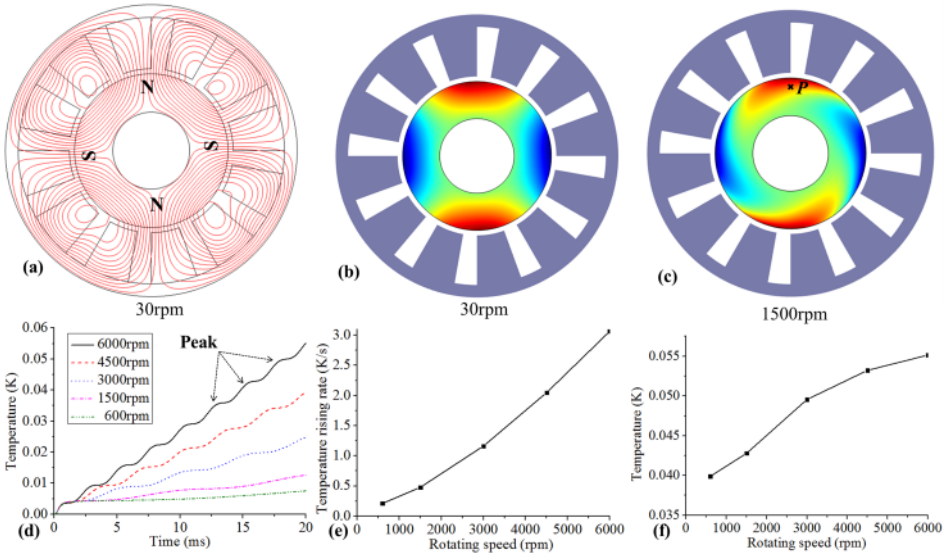

FIG. 2. Numerical simulation for MIEC induced by rotating magnetic field. (a) Magnetic flux distributions at speed of 30rpm; (b) and (c) The MIEC distributions in the specimen at different rotating speeds of 30rpm and 1500rpm, respectively; (d) The temperature rise with different rotating speeds; (e) Temperature rising rates for different rotating speeds; (f) The temperature at point P for the same number of pulsed MIEC.

Further, the temperature at point P (Depth:1.0 mm) is simulated at specified rotating speeds of 600rpm, 1500rpm, 3000rpm, 4500rmp and 6000rpm, as displayed in Fig. 2(d). It can be seen that due to the enhanced MIEC density a higher rotating speed will generate a higher temperature rising rate. The relationship between temperature rising rate and rotating speed is calculated and displayed in Fig. 2 (e), which shows an increasing trend of temperature rising rate with respect to the rotating speed.

On the other hand, as displayed in Fig. 2(d), during the heating process, series of temperature peaks are generated. With the magnetic field rotating for one revolution, there will be four pulsed MIEC scanning the point P, and the point will be heated and cooled for four times, leading to the temperature peaks. For on-line monitoring of the rail track, a feasible heating device of MIECT is

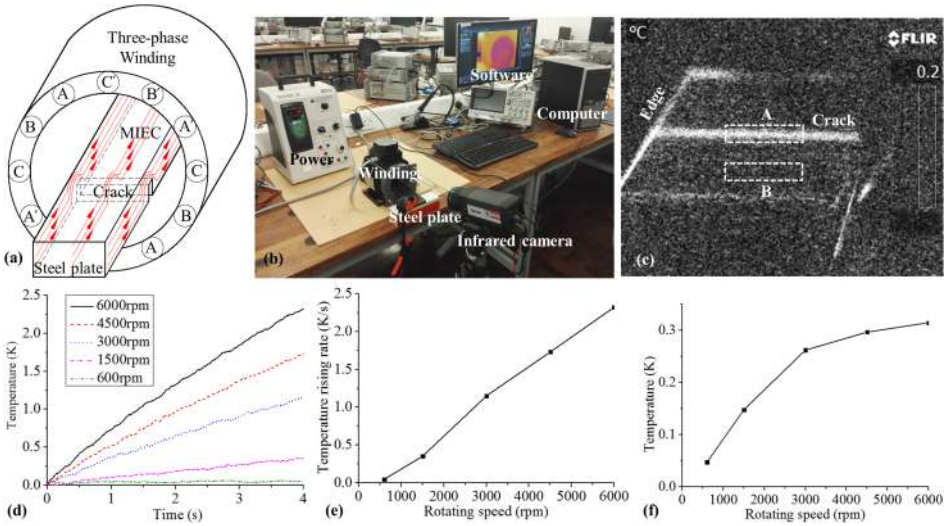

FIG. 3. MIECT experiment based on an electronic-driven rotating magnetic field. (a) MIECT experimental schematic diagram; (b) Experimental setup; (c) The thermal image on the steel plate surface; (d) The temperature rise with different rotating speeds; (e) Temperature rising rates for different rotating speeds; (f) The thermal contrasts with the same number of pulsed MIEC.

linearly-arranged permanent magnet array. A fixed number of magnets will generate the same number of pulsed MIEC to scan the defect. To investigate the heating principle of the permanent magnet array, the relevant heating time for the rotating speeds of 600rpm, 1500rpm, 3000rpm, 4500rpm and 6000rpm are respectively set as 200ms, 80ms, 40ms, 26.7ms, and 20ms to generate the same number of pulsed MIEC. Fig. 3(f) shows the temperature of the point P after the specimen is heated for above-set time. It can be seen that for the permanent magnet array, the scanning speed will also enhance the heating efficiency; however, when the scanning speed reaches to a high level, the enhance effect becomes weak, thus an optimal speed will be reached.

IV. EXPERIMENTAL STUDIES

To validate the feasibility of the proposed MIECT method, experimental study based electronic-driven rotating magnetic field is conducted. In order to obtain an open view for the infrared camera, a steel plate (Width: 50.0 mm; Thickness: 10.0 mm) is tested with an artificial circumferential crack (Width: 3.0 mm; Depth: 8.0 mm), as displayed in Fig. 3(a). The crack will block the flow of axially-oriented MIEC and result in a higher temperature. As pictured in Fig. 3 (b), the windings are driven by three-phase currents power (Current Intensity: 10A) with different frequencies to generate different rotating speeds. Temperature distribution on the plate surface is captured by infrared camera Flir SC655A. Fig. 3 (c) shows the thermal image after the plate is heated for 0.4s with the rotating speed of 6000rpm. It can be seen that the defect area shows higher temperature response than the defect-free area. In the experiment, thermal contrast ΔT between defective and defect-free areas, which reflects the heating efficiency, is analyzed[22]

$$\Delta T = T_A - T_B \tag{8}$$

where T_A and T_B denote the average temperatures at defective area A and defect-free area B, respectively, as displayed in Fig. 3(c).

Firstly, the influence of the rotating speed on the thermal contrast is investigated. By changing the three-phase current frequency, the windings create magnetic fields with specified rotating speeds of 600rpm, 1500rpm, 3000rpm, 4500rpm and 6000rpm. Fig. 3 (d) shows the thermal contrast rise at different rotating speeds. It can be seen that a higher rotating speed will generate a higher temperature increasing rate, and their relationship are calculated and displayed in Fig. 3(e), which matches the simulation results well, as displayed in Fig. 2(e).

To validate the heating principle of the linearly-arranged permanent magnet array, for different rotating speeds of 600rpm, 1500rpm, 3000rpm, 4500rpm and 6000rpm, the relevant heating time are respectively set as 4.0 s, 1.6 s, 0.8 s, 0.53 s, and 0.4 s to generate the same number of pulsed MIEC. Fig. 3(f) shows the thermal contrast at the end of the heating for above-set time. It can be seen that with a fixed number of pulsed MIEC, increasing the scanning speed will improve the thermal contrast; however, when the moving speed reaches to a high level, thermal contrast rise is slowing down, which agrees with the simulation results as displayed in Fig. 2(f).

Besides, in the experiment at the defect position, for rotating speeds from 600rpm to 6000rpm, the rotational velocity is approximate from 8 km/h to 80 km/h, thus, the experiment results preliminarily validate that the proposed MIECT method is a platform suitable for high-speed inspection, such as on-line monitoring for rail track and wheel.

V. CONCLUSION AND FUTURE WORKS

In this letter, a novel motion-induced eddy current based thermography method is proposed for high-speed inspection, and its feasibility study is investigated by a rotating magnetic field created by electronic-driven way. Simulation and experimental results preliminarily validate that the moving speed will increase MIEC intensity and thereafter improve the heating efficiency. Besides, with a fixed number of pulsed MIEC, increasing the scanning speed will enhance the heating efficiency; however, when the scanning speed reaches to a high level, the enhance effect becomes weak, thus an optimal speed will be reached. In future work, the influence of the defect characteristics on the thermal contrast will be studied, and a permanent magnet array scanning system for the optimal speed will be developed and evaluated.

ACKNOWLEDGMENTS

This work was financially supported by EPSRC EP/K503885/1, UK and National Natural Science Foundation of China (Grant No. 51505308, 51377015, 61527803), the Fundamental Research Funds for the Central Universities (Grant No. 2015SCU11059) and China Scholarship Council (Grant No. 201606245039).

[1] X. Maldague and S. Marinetti, J. Appl. Phys. **79**(5), 2694–2698 (1996).
[2] N. Tabatabaei, A. Mandelis, and B. T. Amaechi, Appl. Phys. Lett. **98**(16), 163706 (2011).
[3] F. Fertig, J. Greulich, and S. Rein, Appl. Phys. Lett. **104**(20), 201111 (2014).
[4] B. Gao, W. L. Woo, and G. Y. Tian, Scientific Reports **6**, 25480 (2016).
[5] R. Yang and Y. He, Appl. Phys. Lett. **106**(23), 234103 (2015).
[6] L. Cheng, B. Gao, G. Y. Tian, W. L. Woo, and G. Berthiau, IEEE Sensors Journal **14**(5), 1655–1663 (2014).
[7] D. Huang, K. Li, G. Y. Tian, A. I. Sunny, X. Chen, C. Tang, J. Wu, H. Zhang, and A. Zhao, Sensors and Actuators A: Physical **251**, 248–257 (2016).
[8] K. Li, G. Y. Tian, L. Cheng, A. Yin, W. Cao, and S. Crichton, IEEE Trans. Power Electr. **29**(9), 5000–5009 (2014).
[9] G. Y. Tian, Y. Gao, K. Li, Y. Wang, B. Gao, and Y. He, Sensors **16**(6), 843 (2016).
[10] U. Netzelmann, G. Walle, A. Ehlen, S. Lugin, M. Finckbohner, and S. Bessert, AIP Conference Proceedings **1706**(1), 150001 (2016).
[11] J. Wu, Y. Sun, B. Feng, and Y. Kang, IEEE Trans. Magn. **53**(7), 6201506 (2017).
[12] Y. Li, G. Y. Tian, and S. Ward, NDT & E Int. **39**(5), 367–373 (2006).
[13] J. Xin, N. Lei, L. Udpa, and S. S. Udpa, NDT & E Int. **54**, 45–55 (2013).
[14] C. Ye, J. Xin, Z. Su, L. Udpa, and S. S. Udpa, IEEE Trans. Magn. **51**(7), 1–6 (2015).
[15] T. J. Rocha, H. G. Ramos, A. L. Ribeiro, and D. J. Pasadas, IEEE Trans. Instrum. Meas. **65**(5), 1182–1187 (2016).
[16] J. B. Nestleroth and R. J. Davis, NDT & E Int. **40**(1), 77–84 (2007).
[17] H. Brauer and M. Ziolkowski, Serbian Journal of Electrical Engineering **5**(1), 11–20 (2008).
[18] M. Fabbri, M. Forzan, S. Lupi, A. Morandi, and P. L. Ribani, IEEE Trans. Magn. **45**(1), 192–200 (2009).
[19] M. Messadi, L. Hadjout, Y. Ouazir, T. Lubin, S. Mezani, A. Rezzoug, and N. Takorabet, IEEE Trans. Magn. **52**(3), 1–4 (2016).
[20] Y. Jin, B. Kou, L. Zhang, H. Zhang, and H. Zhang, in Proceedings of 19th International Conference on Electrical Machines and Systems, (IEEE, Chiba, Japan, 2016).
[21] X. Lu, Y. Li, M. Wu, J. Zuo, and W. Hu, Journal of Traffic and Transportation Engineering (English Edition) **1**(6), 448–456 (2014).
[22] Y. Gao, G. Y. Tian, P. Wang, H. Wang, B. Gao, W. L. Woo, and K. Li, Sci. Rep. **7**, 42073 (2017).